bioRxiv preprint doi: https://doi.org/10.1101/2025.02.01.636075; this version posted February 2, 2025. The copyright holder for this preprint (which was not certified by peer review) is the author/funder, who has granted bioRxiv a license to display the preprint in perpetuity. It is made available under aCC-BY-NC-ND 4.0 International license.

Shigella OspF blocks rapid p38-dependent priming of the NAIP–NLRC4 inflammasome

Elizabeth A. Turcotte[1], Kyungsub Kim[2], Kevin D. Eislmayr[1], Lisa Goers[2], Patrick S. Mitchell[3,4], Cammie F. Lesser[2,5,6,7]*, Russell E. Vance[1,8,9,10]*

[1]Division of Immunology & Molecular Medicine, Department of Molecular & Cell Biology, University of California, Berkeley, United States
[2]Department of Microbiology, Harvard Medical School, Boston, United States
[3]Department of Microbiology, University of Washington, Seattle, United States
[4]Howard Hughes Medical Institute, University of Washington, Seattle, United States
[5]Broad Institute of Harvard and MIT, Cambridge, United States
[6]Department of Medicine, Division of Infectious Diseases, Massachusetts General Hospital, Boston, United States
[7]Department of Molecular Biology and Microbiology, Tufts University School of Medicine, Boston, United States
[8]Center for Emerging and Neglected Disease, University of California, Berkeley, United States
[9]Cancer Research Laboratory, University of California, Berkeley, United States
[10]Howard Hughes Medical Institute, University of California, Berkeley, United States

*co-corresponding author

Abstract

The NAIP–NLRC4 inflammasome senses pathogenic bacteria by recognizing the cytosolic presence of bacterial proteins such as flagellin and type III secretion system (T3SS) subunits. In mice, the NAIP–NLRC4 inflammasome provides robust protection against bacterial pathogens that infect intestinal epithelial cells, including the gastrointestinal pathogen *Shigella flexneri*. By contrast, humans are highly susceptible to *Shigella*, despite the ability of human NAIP–NLRC4 to robustly detect *Shigella* T3SS proteins. Why the NAIP–NLRC4 inflammasome protects mice but not humans against *Shigella* infection remains unclear. We previously found that human THP-1 cells infected with *Shigella* lose responsiveness to NAIP–NLRC4 stimuli, while retaining sensitivity to other inflammasome agonists. Using mT3Sf, a “minimal *Shigella*” system, to express individual secreted *Shigella* effector proteins, we found that the OspF effector specifically suppresses NAIP–NLRC4-dependent cell death during infection. OspF was previously characterized as a phosphothreonine lyase that inactivates p38 and ERK MAP kinases. We found that p38 was critical for rapid priming of NAIP–NLRC4 activity, particularly in cells with low NAIP–NLRC4 expression. Overall, our results provide a mechanism by which *Shigella* evades inflammasome activation in humans, and describe a new mechanism for rapid priming of the NAIP–NLRC4 inflammasome.

Introduction

Inflammasomes are cytosolic sensors of pathogen ligands, pathogen activities, and other noxious stimuli. Upon triggering, inflammasomes recruit and activate caspases that induce cell death and the release of the proinflammatory cytokines interleukin (IL)-18 and IL-1β. The NAIP–NLRC4 inflammasome is activated upon NAIP recognition of specific bacterial proteins, including flagellin, or the rod or needle proteins of bacterial type III secretion systems (T3SS) (*1-5*). A single ligand-bound NAIP assembles with multiple copies of NLRC4 (*6, 7*), which then recruit and activate Caspase-1, a protease that processes pro-IL-18 and pro-IL-1β into their active forms. Caspase-1 also cleaves and activates Gasdermin-D (GSDMD), a pore forming

bioRxiv preprint doi: https://doi.org/10.1101/2025.02.01.636075; this version posted February 2, 2025. The copyright holder for this preprint (which was not certified by peer review) is the author/funder, who has granted bioRxiv a license to display the preprint in perpetuity. It is made available under aCC-BY-NC-ND 4.0 International license.

protein that initiates pyroptotic cell death (*8, 9*). Another inflammatory caspase, Caspase-4, forms a 'non-canonical' inflammasome upon direct recognition of cytosolic LPS. Active Caspase-4 also cleaves GSDMD to induce pyroptosis (*10, 11*). Pyroptosis is important for eliminating infected cells, and for inducing a proinflammatory response to halt infection.

Shigella spp. are Gram-negative bacteria that are the causative agents of shigellosis, a diarrheal disease that disproportionately affects young children in low and middle income countries. *Shigella* causes more than 250 million cases and over 200,000 deaths each year (*12*). *Shigella* are human-specific pathogens that are transmitted via the fecal-oral route and cause disease by invading and replicating within intestinal epithelial cells (IECs). Successful infection requires a plasmid-encoded T3SS which facilitates the cytosolic delivery of >20 bacterial effectors into host cells (*13*).

Although wild-type mice are highly resistant to oral *Shigella* infection, we recently established the first mouse model of infection that uses a physiological oral route of infection (*14*). This model was established by the genetic elimination of the NAIP–NLRC4 inflammasome, which is highly expressed in mouse intestinal epithelial cells and acts as a potent barrier to *Shigella* infection. Despite the ability of human NAIP–NLRC4 to sense the *Shigella* T3SS needle (MxiH) and rod (MxiI) proteins (*4, 5, 14*) humans are not protected from infection. One reason for this may be the apparently low expression of NAIP–NLRC4 in human intestinal epithelial cells (*15*). However, we previously found that the NAIP–NLRC4 inflammasome is suppressed by *Shigella* infection in human THP-1 cells (*14*). *Shigella* uses many effectors to suppress host immune responses. For example, *Shigella* OspC3 inactivates human CASP4 by ADP-riboxanation (*16, 17*), and *Shigella* IpaH9.8 degrades anti-bacterial guanylate-binding proteins (*18-21*). Thus, we hypothesized that *Shigella* might encode an effector that suppresses the NAIP–NLRC4 inflammasome.

In order to test if a secreted *Shigella* effector could suppress NAIP–NLRC4, we screened *Shigella* strains expressing individual effectors. This screen identified OspF as a specific suppressor of NAIP–NLRC4. OspF was previously described as a phosphothreonine lyase that irreversibly inactivates MAP kinases such as p38 and ERK (*22-24*). We found that p38 can rapidly prime NAIP–NLRC4, independent of new transcription and translation, and that OspF inhibits p38-dependent priming of NAIP–NLRC4. These effects were particularly important in cells with low expression of NAIP–NLRC4. Our results identify a new mechanism of rapid priming of the NAIP–NLRC4 inflammasome, and provide a mechanism by which *Shigella* could evade host immunity provided by NAIP–NLRC4.

Results

A mT3Sf screen identifies OspF as a specific suppressor of the NAIP–NLRC4 inflammasome

The T3SS and almost all *Shigella* effectors are encoded on a large 220kB virulence plasmid (*25*). mT3Sf is a virulence-plasmid minus variant of *S. flexneri* that contains operons that encode the components needed to form the type III secretion apparatus (T3SA) and four embedded effectors (IpgB1, IpaA, IcsB, IpgD), plus a plasmid that encodes their shared transcriptional regulator VirB under the control of the P_{Tac} IPTG-inducible promoter. In this background, each mT3Sf strain also harbors a unique plasmid encoding a single effector, or empty vector (Kim et al, in preparation). These strains express a functional T3SS and are capable of invading and escaping into the cytosol of infected epithelial cells (Kim et al, in preparation). mT3Sf retain the potential to activate the NAIP–NLRC4 inflammasome (via the T3SS rod and needle proteins) and CASP4 (via cytoplasmic LPS) (Figure 1A). Thus, we set out to use the mT3Sf strains to conduct a screen to study the roles of individual effectors in a bottom-up platform where the NAIP–NLRC4 and CASP4 inflammasomes are activated naturally

bioRxiv preprint doi: https://doi.org/10.1101/2025.02.01.636075; this version posted February 2, 2025. The copyright holder for this preprint (which was not certified by peer review) is the author/funder, who has granted bioRxiv a license to display the preprint in perpetuity. It is made available under aCC-BY-NC-ND 4.0 International license.

by infection, free of the confounding effects of additional effectors that may normally suppress these inflammasomes or activate others.

Infection with mT3Sf::empty induced cell death of infected THP-1 human macrophages, that was eliminated in *NLRC4*$^{-/-}$*CASP4*$^{-/-}$ double knockout cells (Figure 1B). As expected, cell death also required GSDMD (Figure 1B). We observed substantial levels of cell death in mT3Sf-infected *CASP4*$^{-/-}$ cells (mediated by NLRC4) and in *NLRC4*$^{-/-}$ cells (mediated by CASP4), confirming that mT3Sf::empty infection induces pyroptosis via activation of both of these two main cell death pathways. To screen for effector(s) that suppress NAIP–NLRC4, we infected *CASP4*$^{-/-}$ THP-1 cells. In these cells infection with mT3Sf strains expressing OspF, IpaH7.8, IpaH1.4, and OspI significantly suppressed cell death relative to mT3Sf::empty (Figure 1C). To assess whether the inhibition was specific for the NAIP–NLRC4 inflammasome, we also screened the mT3Sf strains in *NLRC4*$^{-/-}$ THP-1 cells (in which cell death is mediated by CASP4). In these cells, we found that OspI, IpaH7.8, IpaH9.8, OspC3, and IpaH1.4 significantly suppressed cell death (Figure 1D).

To identify inhibitors specific for either NLRC4 or CASP4, we calculated the ratio of the cell death between CASP4- and NLRC4-deficient cells for each individual mT3Sf::effector strain (Figure 1E). This analysis revealed that some inhibitory effectors non-specifically suppressed both NLRC4- and CASP4-induced cell death (resulting in a cell death ratio close to 1) (Figure 1E). These effectors include IpaH7.8, which ubiquitylates and thereby induces the degradation of GSDMB and GSDMD (*26-28*), as well as IpaH1.4 and OspI, which interfere with NF-κB signaling (*29-31*). By contrast, OspC3 and IpaH9.8 specifically suppressed CASP4-dependent death in NLRC4-deficient cells, as expected (*16-21, 32*). Conversely, NLRC4-dependent cell death was specifically and most strongly suppressed by OspF. In addition to suppressing cell death, infection with mT3Sf::OspF also prevented IL-1β processing as compared to mT3Sf::empty (Supp. Figure 1). Infection with the mT3Sf::OspF strain also suppressed NLRC4-dependent IL-1β processing induced by the synthetic NAIP–NLRC4 agonist NeedleTox. NeedleTox has been previously described (*3, 33, 34*) and consists of the T3SS needle protein fused to the N-terminal signal sequence of *Bacillus anthracis* lethal factor (LFn). LFn has no enzymatic or toxic activity, but serves to direct the LFn-Needle fusion protein into the cytosol of host cells via the co-delivered protective antigen (PA) channel-forming protein. In contrast, OspF did not block the ability of nigericin to activate NLRP3 (Supp. Figure 1). Taken together, our screen with the mT3Sf strains lead us to conclude that OspF can specifically suppress NAIP–NLRC4 inflammasome activation during infection.

OspF suppresses the NAIP–NLRC4 inflammasome during *Shigella* infection via p38 inactivation in human cells

We tested the role of OspF during infection with virulent *Shigella* by infecting THP-1 cells with wild-type (WT), Δ*ospF,* and Δ*ospF*+ospF plasmid complemented *Shigella* strains. Cells infected with the Δ*ospF* mutant showed enhanced cell death compared to WT-infected cells (Figure 2A). Furthermore, this enhanced cell death was entirely NLRC4-dependent as it was absent in *NLRC4*$^{-/-}$ cells (Figure 2A). *CASP4*$^{-/-}$ cells with intact NAIP–NLRC4 responses also showed enhanced cell death upon infection with Δ*ospF Shigella*. Complementation with plasmid-encoded OspF fully reversed the enhanced death seen with Δ*ospF* (Figure 2A).

OspF is a phosphothreonine lyase that irreversibly removes the phosphorylated hydroxyl moiety from activated mitogen activated protein kinases (MAPKs) by beta elimination (*22*), with specificity for p38 and ERK1/2 (*23, 24*). To determine if suppression of NLRC4 depends on the same features of OspF that confer its specificity for MAPKs, we complemented Δ*ospF* with a plasmid expressing an OspF KLA (“KLA”) mutant, which has mutated lysine and leucine residues to alanine in the N-terminal D-domain that is essential for recognition of MAPK substrates (*35*). We found that the OspF KLA mutant was unable to reverse the enhanced cell

bioRxiv preprint doi: https://doi.org/10.1101/2025.02.01.636075; this version posted February 2, 2025. The copyright holder for this preprint (which was not certified by peer review) is the author/funder, who has granted bioRxiv a license to display the preprint in perpetuity. It is made available under aCC-BY-NC-ND 4.0 International license.

death seen with the Δ*ospF* mutant (Figure 2B). This result indicates that the D-domain is required for OspF suppression of NAIP–NLRC4. We also complemented *Shigella* Δ*ospF* with a plasmid expressing the *Salmonella* OspF homolog, SpvC, which also is a phosphothreonine lyase that targets MAP kinases (*35, 36*). SpvC fully reversed the enhanced cell death produced by infection with the Δ*ospF* mutant (Figure 2B). Thus, inhibition of NLRC4 correlates with inhibition of MAPK, and the most parsimonious explanation of our results is that inhibition of NLRC4 is via the known ability of OspF to inhibit MAPK. However, it is also possible OspF acts on other substrates.

To assess if OspF acts via MAPK inhibition, we investigated whether MAPKs are involved in NAIP–NLRC4 activation upon *Shigella* infection. We assayed the induction of phospho-p38 and phospho-ERK1/2 in infected *GSDMD*$^{-/-}$ cells (Figure 2C). In these experiments we used *GSDMD*$^{-/-}$ cells to eliminate the confounding effects of rapid pyroptotic cell death. Consistent with previous work, infection with WT, OspF-complemented, or SpvC-complemented *Shigella* efficiently prevented p38 and ERK1/2 phosphorylation, whereas Δ*ospF*, KLA complemented, or avirulent (virulence plasmid-cured) BS103 *Shigella* triggered robust MAPK phosphorylation (Figure 2C). To more directly assess the role of MAPK in NLRC4 activation, we tested whether MAPK inhibitors blocked *Shigella*-induced NLRC4 activation. We found that three different p38 inhibitors (PD169316, SB203580, and TAK715) all prevented NAIP–NLRC4-dependent cell death during Δ*ospF* infection (Figure 2D), whereas use of Mirdametinib to inhibit MEK1/2 upstream of ERK1/2 had no effect (Figure 2E). Furthermore, delivery of *Bacillus anthracis* lethal factor, which cleaves and inactivates MAPK kinases MKK3 and MKK6 upstream of p38 (*37-40*), eliminated p38 phosphorylation (Supp. Figure 2A) and prevented NAIP–NLRC4 activation by the Δ*ospF* mutant (Supp. Figure 2B). Taken together, these results suggest that OspF suppresses NAIP–NLRC4 indirectly via inactivation of p38 MAPK.

Rapid priming sensitizes the NAIP–NLRC4 inflammasome in a p38-dependent manner

Our data imply that p38 signaling positively regulates NAIP–NLRC4 inflammasome activation during infection. To test this, we activated p38 using ligands for pattern recognition receptors that are engaged during *Shigella* infection (*41-45*). Activation of TLR2 by Pam3CSK4, or activation of ALPK1 with ADP-L-Heptose, resulted in robust phospho-p38 in THP-1 cells within 30 minutes (Supp. Figure 3A, B). Infection of THP-1 cells with avirulent BS103 also induced a strong phospho-p38 response (Supp. Figure 3A). Priming THP-1 cells for just 1 hour before treatment with NeedleTox resulted in a significantly enhanced cell death response compared to unprimed cells (Figure 3C). Primed cells responded more quickly than unprimed cells, with significant levels of cell death after just 1 hour of challenge (Figure 3A). Primed cells also responded to a low dose of NeedleTox (10 ng/mL LFn-Needle) to which unprimed cells were unresponsive (Figure 3A, B). As expected, the response of primed cells to NeedleTox was entirely NLRC4-dependent (Figure 3A, B).

We found significantly enhanced responses downstream of all ligands that induced a strong phospho-p38 response, including Pam3CSK4, ADP-L-Heptose (Figure 3), and the NOD1 ligand C12-iE-DAP (Supp. Figure 3D, E). We also confirmed, as expected, that priming induced by Pam3CSK4 depended on TLR2 and MYD88, whereas priming induced by ADP-L-Heptose depended on ALPK1, and priming induced by C12-iE-DAP depended on NOD1 (Supp. Figure 3C-E). Infection with the virulence plasmid-cured BS103 *Shigella* strain primed the NAIP–NLRC4 inflammasome in a TLR2- and MYD88-dependent manner (Supp. Figure 3B, C). We cannot test how virulent *Shigella* primes NLRC4 since virulent *Shigella* itself induces rapid cell death, but we expect TLR2 ligands to be produced similarly by BS103 and virulent *Shigella*. Furthermore, virulent *Shigella* activates additional sensors, such as NOD1 and ALPK1, which can act redundantly with TLR2 to prime NAIP–NLRC4.

bioRxiv preprint doi: https://doi.org/10.1101/2025.02.01.636075; this version posted February 2, 2025. The copyright holder for this preprint (which was not certified by peer review) is the author/funder, who has granted bioRxiv a license to display the preprint in perpetuity. It is made available under aCC-BY-NC-ND 4.0 International license.

Priming of NLRC4 was entirely dependent on p38, as p38 inhibition completely prevented enhanced cell death upon NeedleTox challenge (Figure 3C, Supp. Figure 4A). Consistent with the Δ*ospF* infection data, inhibition of ERK1/2 with Mirdametinib had no effect on priming (Supp. Figure 4B). Notably, p38 is not required for NAIP–NLRC4 activation, nor does p38 inhibition suppress the NeedleTox responses in unprimed cells (Figure 3C, Supp. Figure 4A). Together, these data suggest that p38 is not strictly required for a NAIP–NLRC4 response, but acute p38-dependent priming greatly sensitizes the NAIP–NLRC4 inflammasome to respond.

Notably, although TLR activation also rapidly primed the NLRP3 inflammasome (as previously reported (*46-49*), ADP-L-Heptose did not rapidly prime NLRP3 (Figure 3C). Nor did p38 inhibitors block rapid NLRP3 priming (Figure 3C). These results indicate that the mechanisms of rapid NLRC4 and NLRP3 priming are distinct. Importantly, priming-enhanced NLRC4-induced cell death was completely blocked by the Caspase-1 inhibitor VX-765 (Supp. Figure 5A), indicating that priming promoted canonical Caspase-1 activation downstream of NLRC4 and was not engaging a different Caspase pathway. Furthermore, despite reports that NLRP3 can play a role in NAIP–NLRC4 responses (*50*), a selective NLRP3 inhibitor MCC950 had no effect on NLRC4 priming, indicating that NLRP3 does not contribute to NLRC4 priming (Supp. Figure 5B).

Rapid priming enhances NAIP–NLRC4 activation in a transcription- and translation-independent manner and alleviates the requirement for ASC

Recent work showed that in mouse macrophages extended (16 hours) TLR priming induces a p38-dependent upregulation of NLRC4 expression, resulting in enhanced sensitivity to NAIP ligands (*51*). However, human macrophages did not show the same TLR-dependent enhancement of NAIP–NLRC4 responses. In agreement with this prior report, we confirmed that overnight priming with Pam3CSK4 had no effect on NAIP–NLRC4 responses in human THP-1 cells (Figure 4A). However, rapid priming for 1 hour or at the time of challenge significantly enhanced NAIP–NLRC4 responses (Figure 4A). Treatment of cells with the translation inhibitor cycloheximide, or the transcription inhibitor actinomycin D, had no effect on rapid priming of the NAIP–NLRC4 inflammasome (Figure 4B), suggesting priming likely occurs via post-translational modification.

Post-translational modifications of inflammasomes have been well-documented (*52*). One inflammasome component that has been shown to be positively regulated by phosphorylation is the ASC adaptor protein that recruits Caspase-1 downstream of several inflammasomes, including NAIP–NLRC4 (*53-56*). To determine if rapid priming of NAIP–NLRC4 requires ASC, we challenged *ASC*$^{-/-}$ THP-1 cells under rapid priming conditions. We found that ASC was required for cell death upon NeedleTox challenge in unprimed THP-1 cells. Interestingly, however, rapid priming with Pam3CSK4 alleviated the requirement of ASC for the response to NeedleTox, and primed *ASC*$^{-/-}$ cells were able to undergo NLRC4-induced pyroptosis (Figure 4C). Thus, ASC is not required for rapid priming of NAIP–NLRC4.

Rapid priming depends on NAIP–NLRC4 levels but not NAIP isoform

We sought to complement our *NLRC4*$^{-/-}$ THP-1 cells with wild-type human NLRC4, expressed using MSCV2.2 retroviral transduction. Interestingly, we found that overexpression of NLRC4 rendered cells extremely responsive to NeedleTox challenge (Figure 5A). The strong response masked our ability to see priming effects, even when we titrated the amount of NLRC4 agonist we used (Figure 5A). Primary human macrophages have been shown to express more NLRC4 and NAIP than THP-1 cells (*57*). Consistent with this result, we found that primary human monocyte-derived macrophages are much more responsive to NeedleTox than THP-1 cells. Again, the high level of responsiveness of primary monocyte-derived macrophages masked the effect of priming in these cells (Figure 5B).

bioRxiv preprint doi: https://doi.org/10.1101/2025.02.01.636075; this version posted February 2, 2025. The copyright holder for this preprint (which was not certified by peer review) is the author/funder, who has granted bioRxiv a license to display the preprint in perpetuity. It is made available under aCC-BY-NC-ND 4.0 International license.

Similar to primary human cells, we also saw no role for priming in wild-type mouse bone marrow-derived macrophages (BMMs) (Figure 5C), a cell type that is also highly responsive to NLRC4 agonists. However, when we tested BMMs derived from *Nlrc4*$^{+/-}$ (heterozygous) mice, which express reduced levels of NLRC4, we found that these macrophages were responsive to rapid priming with both Pam3CSK4 and ADP-L-Heptose (Figure 5C). This result suggests that rapid priming is a property of both mouse and human cells, but is apparent only in cells expressing lower NLRC4 levels (THP-1 or mouse *Nlrc4*$^{+/-}$ BMMs) while being masked in primary cells expressing higher levels of NLRC4.

To test if human cells expressing mouse NAIPs could be primed, we used retroviral transduction to express mouse *Naip1* and *Naip2* in *NAIP*$^{-/-}$ THP-1 cells (Figure 5D). Mouse NAIP1 detects T3SS Needle and is responsive to NeedleTox (*58*), whereas mouse NAIP2 detects T3SS rod and is unresponsive to NeedleTox, but is responsive to RodTox (*3*). THP-1 cells expressing mouse *Naip1* or *Naip2* in place of human NAIP were still regulated by rapid priming (Figure 5D). This result is consistent with the rapid priming we see in mouse *Nlrc4*$^{+/-}$ BMMs and confirm that both human and mouse NAIP proteins can form rapidly primed NAIP–NLRC4 inflammasomes. Furthermore, although overexpression of NLRC4 prevented us from seeing the priming effect, cells overexpressing NAIP1 or NAIP2 were still rapidly primed, similar to WT THP-1 cells, suggesting that NLRC4 levels determine the sensitivity to priming.

Discussion

Humans are highly susceptible to *Shigella* infection, whereas mice are resistant due to the potent protection afforded by the NAIP–NLRC4 inflammasome. We previously found that NAIP–NLRC4 is actively suppressed during infection of human THP-1 cells (*14*). Here we found that in human THP-1 cells, NAIP–NLRC4 is suppressed during infection by the secreted effector OspF. Infection with Δ*ospF* resulted in significantly enhanced cell death that depended on both NAIP–NLRC4 and p38 MAP kinases. Our data suggest that the link between p38 and NAIP–NLRC4 activation during *Shigella* infection involves the rapid post-translational priming of NAIP–NLRC4. Treatment of cells for 1 hour or less with innate immune agonists that active p38 resulted in significantly enhanced responses to a NAIP–NLRC4 agonist. Rapid priming required p38 activity, and occurred in the presence of transcription and translation inhibitors, suggesting it occurs post-translationally.

Phosphorylation of NLRC4 at serine 533 (S533) has been proposed to stimulate NAIP–NLRC4 activation. This site has been primarily studied in mice, and its importance for human NAIP–NLRC4 function is unclear (*59-62*). Previous studies identified PKCδ and LRRK2 as putative kinases regulating phosphorylation of S533 (*59, 61, 63*), though the role of PKCδ is controversial (*64*). S533 has not been proposed to be a site of p38 MAPK phosphorylation. Nevertheless, it is possible that S533 phosphorylation contributes to the observed rapid priming of NAIP–NLRC4. Our attempts to use mass spectrometry to identify additional NLRC4 phosphorylation sites have thus far been inconclusive.

Notably, we found that unprimed THP-1 cells required ASC for cell death induced by the NeedleTox NAIP–NLRC4 agonist; however, priming with Pam3CSK4 alleviated the requirement for ASC (Figure 4C). NLRC4 lacks a PYD, but contains a CARD which is capable of direct interaction with the CARD of Caspase-1 (*65*). Although ASC is generally required for Caspase-1 activation by PYD-containing inflammasomes, the NAIP–NLRC4 inflammasome can induce cell death in the absence of ASC (*66-69*). Whether ASC is required for NAIP–NLRC4 activation in human cells is not clear. However, it was shown that in the context of *Salmonella* infection in primary human macrophages, ASC is required for cytokine processing but dispensable for pyroptosis, in line with mouse data (*70*). Consistent with our results, Moghaddas, et al showed that in THP-1 cells, ASC was largely required for both cell death and cytokine response to the

bioRxiv preprint doi: https://doi.org/10.1101/2025.02.01.636075; this version posted February 2, 2025. The copyright holder for this preprint (which was not certified by peer review) is the author/funder, who has granted bioRxiv a license to display the preprint in perpetuity. It is made available under aCC-BY-NC-ND 4.0 International license.

T3SS needle protein PrgI (delivered by a retroviral expression vector) (*71*). In this system, cells were primed with Pam3CSK4 for 3 hours before infection with PrgI-expressing retrovirus, and cell death and cytokine release were measured after 24 hours. Under these conditions, a requirement for ASC was still observed, consistent with our finding that the priming effect on NAIP–NLRC4 is a rapid and transient event.

One important future area for study is to identify the physiological context in which rapid priming of NAIP–NLRC4 might be important. *Shigella* invades and forms its replicative niche in IECs, and in mice, NAIP–NLRC4 in IECs is essential for protection from *Shigella* infection (*14, 72*). Moreover, NAIP–NLRC4 in mouse IECs has also been shown to be an important contributor for protection against other enteric pathogens (*73-75*). However, mouse IECs express especially high levels of NLRC4 and NAIPs compared to other cell types, thus potentially masking p38-mediated priming of NLRC4 (*76*). In contrast, it has been reported that NAIP and NLRC4 is expressed at low or undetectable levels in human intestinal organoids or epithelial cell lines (*15, 77*). However, expression in human epithelial cells within the gut during infection or inflammation may be distinct from those observed *in vitro*. Indeed, humans with gain-of-function NLRC4 mutations often show gastrointestinal pathology (*71, 78-82*), suggesting that NLRC4 may function in the gut *in vivo* in some contexts. Thus, rapid priming may promote inflammasome activation in human epithelial cells. Regardless, our finding that NAIP–NLRC4 responsiveness can be enhanced by rapid p38-dependent priming adds significantly to our understanding of the regulation of this important inflammasome. The ability of priming to overcome the loss of ASC suggests that priming might be especially critical in the context of a pathogen that inhibits ASC. Moreover, the rapidity and transient nature of the priming suggests that NAIP–NLRC4 may have evolved as a “coincidence detector” in which maximal responsiveness only occurs when the priming (e.g., TLR) signal is coincident with the cytosolic presence of the NAIP ligand (e.g., T3SS Needle). We speculate that such coincidence detection may provide a mechanism to respond preferentially to stimuli—such as infection with a virulent T3SS+ pathogen—that provide both signals within a narrow spatiotemporal window.

Methods

Cell Culture

THP-1 cells were maintained in RPMI with 10% FBS, 100 U/mL penicillin, 100 mg/mL streptomycin, and 2 mM L-glutamine. THP-1 cells were differentiated in 100 ng/mL phorbol myristate acetate (PMA, Invivogen, tlrl-pma) for 48 hr, followed by a 36 hr rest without PMA or antibiotics before use for challenge or infection. THP-1 cells were purchased from ATCC. GP2-293 cells (Clontech) were grown in DMEM with 10% FBS, 100 U/mL penicillin, 100 mg/mL streptomycin, and 2 mM L-glutamine. Primary B6 BMMs were generated by collecting leg bones from WT, *Nlrc4*$^{+/-}$ and *Nlrc4*$^{-/-}$ and crushed by mortar and pestle. Bone marrow was filtered through a 70 µm strainer and treated with ACK lysing buffer (Gibco). Cells were differentiated for 7 days in RPMI supplemented with 10% FBS, 10% 3T3-MCSF supernatant, 100 U/mL penicillin, 100 mg/mL streptomycin, and 2 mM L-glutamine. BMMs were harvested in cold PBS and replated for experiments. De-identified primary human monocytes were purchased from AllCells. Cryopreserved negatively selected monocytes were thawed and seeded for differentiation in RPMI containing 10% FBS, 10 0U/mL penicillin, 100 mg/mL streptomycin, and 2 mM L-glutamine, with 50 ng/mL human M-CSF (PeproTech, 300-25) for 6 days. Cells were collected in trypsin and replated for experiments.

Bacterial Strains

Experiments were conducted using the WT *S. flexneri* serovar 2a 2457T strain. BS103 is a virulence plasmid-cured strain derived from the WT strain (*83*). Δ*ospF* and Δ*ospF*+OspF were described previously (*24*). OspF KLA mutant and *Salmonella typhimurium* SpvC were cloned

bioRxiv preprint doi: https://doi.org/10.1101/2025.02.01.636075; this version posted February 2, 2025. The copyright holder for this preprint (which was not certified by peer review) is the author/funder, who has granted bioRxiv a license to display the preprint in perpetuity. It is made available under aCC-BY-NC-ND 4.0 International license.

into pAM238, and are under the control of the OspF promoter via overlap PCR. Complemented strains were grown in presence of spectinomycin.

Strains used are listed in Supplemental Table 1.

Shigella Infections

Overnight cultures of *Shigella* were grown in 3 mL TSB at 37°C, 220 rpm. On the day of infection *Shigella* cultures were diluted 1:100 in 5 mL TSB and grown for 2-2.5 hr at 37°C until reaching an OD of 0.6-0.8. The bacteria were pelleted and washed 3x with warm complete RPMI without Pen/Strep. Bacteria were added to cells and spun at 400 x*g*, for 10 min at 37°C to synchronize infection. The plates were then incubated at 37°C for 10m before replacing the media with media containing 100 µg/mL propidium iodide (PI) (Sigma) and 100 µg/mL gentamicin (Gibco). PI uptake was measured using a Tecan Spark plate reader. Cell death was calculated relative to 1% Triton X-100-treated wells as 100% cell death, and all subtracted background from media only controls.

Cultures of mT3Sf were grown and used for infection as with WT *Shigella*, except on the day of infection, mT3Sf were diluted 1:100 in 5 mL TSB and grown for 1 hr. After 1 hr, cultures were supplemented with IPTG (1 mM) and returned to 37°C, 220 rpm until grown for a total of 2.5-3 hr.

CRISPR-Cas9 Targeting in THP-1s

THP-1 KO lines were generated as described (*84*). In brief, THP-1 cells were electroporated with a plasmid U6-sgRNA-CMV-mCherry-T2A-Cas9 plasmid using a Biorad Gene Pulser Xcell. 20h after electroporation, mCherry-positive cells were sorted on the BD FACSAria sorter. Sorted cells were plated at limiting dilution in order to acquire a single cell per well. After 2-3 weeks, clones were selected and submitted for MiSeq. Outknocker analysis was performed and clones with out-of-frame indels were selected for use. Guide sequences were designed using CHOPCHOP (*85*) and are as follows: *NLRC4* gRNA target site: 5′-ATCGTGTGAGCAGTGATGGATGG-3′; *CASP4* gRNA target site: 5′-GCCACTGAAAGATACATACGTGG-3′; *GSDMD* gRNA target site: 5′-GCATGGGGTCGGCCTTTGAGCGG-3′; *NAIP* gRNA target site: 5′-ACATTGCCAAGTACGACATAAGG-3′; *ASC* gRNA target site: 5′-ACCGGGCTGCGCTTATCGCGAGG-3′; *TLR2* gRNA target site: 5′-TGGAAACGTTAACAATCCGGAGG-3′; *MYD88* gRNA target site: 5′-GGTTGAGCTTACCTGGAGAGAGG-3′; *ALPK1* gRNA target site: 5′-GTTGGAAGCGCCAGATGTGTCGG-3′; *NOD1* gRNA target site: 5′-ATCTCAACGACTACGGCGTGCGG-3′. *CASP4/NLRC4*$^{-/-}$ and *GSDMD/NLRC4*$^{-/-}$ were generated on the *CASP4*$^{-/-}$ and *GSDMD*$^{-/-}$ background, respectively, using the same NLRC4 gRNA as for the *NLRC4*$^{-/-}$.

Retroviral Transduction

GP2-293 cells were reverse-transfected with Lipofectamine 2000 (Invitrogen), 0.8µg VSV-G and 1.7µg MSCV2.2-IRES-GFP construct. After 18h, the media was changed to THP-1 media. 48h after media change, the GP2 media was syringe-filtered with a 45µM filter over THP-1 cells, and 10 µg/mL protamine sulfate was added. Cells were spun at 1000 x*g* for 1 hr, at 32°C. Transduced cells were expanded and sorted on the BD FACSAria sorter for GFP-positive cells 3-4 days post transduction. MSCV2.2-hNLRC4-HA, MSCV2.2-mNaip1, and MSCV2.2-mNaip2 have been described previously (*3, 14*).

Cell Treatment and Inhibitor Conditions

bioRxiv preprint doi: https://doi.org/10.1101/2025.02.01.636075; this version posted February 2, 2025. The copyright holder for this preprint (which was not certified by peer review) is the author/funder, who has granted bioRxiv a license to display the preprint in perpetuity. It is made available under aCC-BY-NC-ND 4.0 International license.

For activating PRRs, cells were treated with 100 ng/mL Pam3CSK4 (Invivogen, tlrl-pms), 100 ng/mL ADP-L-Heptose (Invivogen, tlrl-adph-l), 100 ng/mL LPS (Enzo, ALX-581-013), or 1 µg/mL C12-iE-DAP (Invivogen, tlrl-c12dap) for the indicated times. Inhibitors were added 1 hr before infection or challenge and were present throughout the experiment. For NLRP3 activation, cells were treated with 5 µg/mL Nigericin (Invivogen, tlrl-nig). Cells were treated with 5 µM PD169316 (MCE, HY-10578), 5 µM SB203580 (SelleckChem, S2928), 5 µM TAK715 (SelleckChem, S1076), 5 µM Mirdametinib (MCE, HY-10254), 20 µM VX-765 (Invivogen, inh-vs765i-1), 10 µM MCC950 (Invivogen, inh-mcc), 250n g/mL cycloheximide (Sigma), or 2 µg/mL Actinomycin D (ThermoFisher).

PA Delivery

Anthrax Lethal Factor protease is delivered into cells via co-administration with protective antigen (PA). Cells were treated with 2 µg/mL PA (List Labs, 171E) only as a control, or 2 µg/mL PA + 1 µg/mL Lethal Factor (List Labs, 169L). Ligands fused to the N-terminal domain of anthrax Lethal Factor (LFn) are able to be translocated into the cytosol only when administered with PA (*3, 33, 34*). For NAIP–NLRC4 activation, the combination of both PA and LFn-Needle or LFn-Rod (known as NeedleTox or RodTox) allows for cytosolic delivery of NAIP–NLRC4 ligands and activation. PA, LFn-Needle or LFn-Rod alone do not induce cell death. Cells were treated with 2 µg/mL PA only, or 2 µg/mL PA + LFn-Needle (Invivogen, tlrl-ndl), or PA + LFn-Rod (Invivogen, tlrl-rod) at the indicated concentrations of LFn proteins.

Cell Death Assays

To measure cell death, 100 µg/mL PI (Sigma) was added at the time of challenge with inflammasome activators. For experiments detecting lactate dehydrogenase (LDH) release, supernatants from were collected and spun to remove any cells or debris. LDH activity was measured with a Cytotoxicity Detection Kit (LDH, Roche). PI uptake or LDH release (Roche) was measured using a Tecan Spark plate reader. Cell death was calculated relative to 1% Triton X-100-treated wells as 100% cell death, and all subtracted background from media only controls.

Western Blot

Whole-cell lysates were prepared by lysis in RIPA buffer (1% NP-40, 0.1% SDS, 0.5% sodium deoxycholate, 50 mM Tris, 150 mM NaCl, 5 mM EDTA) with freshly supplemented HALT protease and phosphatase inhibitor cocktail (ThermoFisher) for 20 min on ice. Lysates were cleared by centrifugation at 18,000x*g* for 20m at 4°C. Laemmli buffer was added (1x final concentration) and boiled for 10 min at 95°C. Samples were separated on NuPAGE Bis-Tris 4-12% gels (ThermoFisher) and transferred onto Immobilon-FL PVDF membranes. Membranes were blocked with Li-Cor Intercept blocking buffer. Primary antibodies were incubated overnight at 4°C. Antibodies used were anti-human IL-1β (R+D, MAB201; 1:1000), anti-vinculin (CST, #13901; 1:1000), anti-phospho-p38 MAPK (CST, #9211; 1:1000), anti-p38 MAPK (CST, #9212; 1:1000), anti-phospho-ERK1/2 MAPK (CST, #4370; 1:1000), and anti-ERK1/2 MAPK (CST, #4695; 1:1000). Secondary Li-Cor IRDye-conjugated antibodies were used at 1:5000. Blots were imaged using Li-Cor Odessey CLx.

Statistical Analysis

Data were analyzed using GraphPad Prism 10. Statistical tests are indicated in the figure legends.

bioRxiv preprint doi: https://doi.org/10.1101/2025.02.01.636075; this version posted February 2, 2025. The copyright holder for this preprint (which was not certified by peer review) is the author/funder, who has granted bioRxiv a license to display the preprint in perpetuity. It is made available under aCC-BY-NC-ND 4.0 International license.

Acknowledgments

This study was funded by National Science Foundation Graduate Research Fellowship Program DGE 1752814 (E.A.T.). R.E.V. is supported by an Investigator Award and an Emerging Pathogens Initiative Award from the Howard Hughes Medical Institute. R.E.V. is also supported by NIH grants AI075039 and AI155634. C.F.L. acknowledges research support from NIH grants AI169795.

Competing Interests

R.E.V. is on the scientific advisory boards of Tempest and X-biotix Therapeutics.

References

1. E. A. Miao *et al.*, Innate immune detection of the type III secretion apparatus through the NLRC4 inflammasome. *Proc Natl Acad Sci U S A* **107**, 3076-3080 (2010).
2. Y. Zhao *et al.*, The NLRC4 inflammasome receptors for bacterial flagellin and type III secretion apparatus. *Nature* **477**, 596-600 (2011).
3. E. M. Kofoed, R. E. Vance, Innate immune recognition of bacterial ligands by NAIPs determines inflammasome specificity. *Nature* **477**, 592-595 (2011).
4. J. Yang, Y. Zhao, J. Shi, F. Shao, Human NAIP and mouse NAIP1 recognize bacterial type III secretion needle protein for inflammasome activation. *Proc Natl Acad Sci U S A* **110**, 14408-14413 (2013).
5. V. M. Reyes Ruiz *et al.*, Broad detection of bacterial type III secretion system and flagellin proteins by the human NAIP/NLRC4 inflammasome. *Proc Natl Acad Sci U S A* **114**, 13242-13247 (2017).
6. L. Zhang *et al.*, Cryo-EM structure of the activated NAIP2-NLRC4 inflammasome reveals nucleated polymerization. *Science* **350**, 404-409 (2015).
7. J. L. Tenthorey *et al.*, The structural basis of flagellin detection by NAIP5: A strategy to limit pathogen immune evasion. *Science* **358**, 888-893 (2017).
8. J. Shi *et al.*, Cleavage of GSDMD by inflammatory caspases determines pyroptotic cell death. *Nature* **526**, 660-665 (2015).
9. N. Kayagaki *et al.*, Caspase-11 cleaves gasdermin D for non-canonical inflammasome signalling. *Nature* **526**, 666-671 (2015).
10. N. Kayagaki *et al.*, Noncanonical inflammasome activation by intracellular LPS independent of TLR4. *Science* **341**, 1246-1249 (2013).
11. J. Shi *et al.*, Inflammatory caspases are innate immune receptors for intracellular LPS. *Nature* **514**, 187-192 (2014).
12. I. A. Khalil *et al.*, Morbidity and mortality due to shigella and enterotoxigenic Escherichia coli diarrhoea: the Global Burden of Disease Study 1990-2016. *Lancet Infect Dis* **18**, 1229-1240 (2018).
13. E. Mattock, A. J. Blocker, How Do the Virulence Factors of. *Front Cell Infect Microbiol* **7**, 64 (2017).
14. P. S. Mitchell *et al.*, NAIP-NLRC4-deficient mice are susceptible to shigellosis. *Elife* **9**, (2020).
15. N. Naseer *et al.*, Salmonella enterica Serovar Typhimurium Induces NAIP/NLRC4- and NLRP3/ASC-Independent, Caspase-4-Dependent Inflammasome Activation in Human Intestinal Epithelial Cells. *Infect Immun* **90**, e0066321 (2022).
16. T. Kobayashi *et al.*, The Shigella OspC3 effector inhibits caspase-4, antagonizes inflammatory cell death, and promotes epithelial infection. *Cell Host Microbe* **13**, 570-583 (2013).

bioRxiv preprint doi: https://doi.org/10.1101/2025.02.01.636075; this version posted February 2, 2025. The copyright holder for this preprint (which was not certified by peer review) is the author/funder, who has granted bioRxiv a license to display the preprint in perpetuity. It is made available under aCC-BY-NC-ND 4.0 International license.

17. Z. Li *et al.*, Shigella evades pyroptosis by arginine ADP-riboxanation of caspase-11. *Nature* **599**, 290-295 (2021).
18. P. Li *et al.*, Ubiquitination and degradation of GBPs by a Shigella effector to suppress host defence. *Nature* **551**, 378-383 (2017).
19. M. P. Wandel *et al.*, GBPs Inhibit Motility of Shigella flexneri but Are Targeted for Degradation by the Bacterial Ubiquitin Ligase IpaH9.8. *Cell Host Microbe* **22**, 507-518.e505 (2017).
20. M. P. Wandel *et al.*, Guanylate-binding proteins convert cytosolic bacteria into caspase-4 signaling platforms. *Nat Immunol* **21**, 880-891 (2020).
21. L. Goers *et al.*, IpaH9.8 limits GBP1-dependent LPS release from intracytosolic bacteria to suppress caspase-4 activation. *Proc Natl Acad Sci U S A* **120**, e2218469120 (2023).
22. H. Li *et al.*, The phosphothreonine lyase activity of a bacterial type III effector family. *Science* **315**, 1000-1003 (2007).
23. L. Arbibe *et al.*, An injected bacterial effector targets chromatin access for transcription factor NF-kappaB to alter transcription of host genes involved in immune responses. *Nat Immunol* **8**, 47-56 (2007).
24. R. W. Kramer *et al.*, Yeast functional genomic screens lead to identification of a role for a bacterial effector in innate immunity regulation. *PLoS Pathog* **3**, e21 (2007).
25. C. Buchrieser *et al.*, The virulence plasmid pWR100 and the repertoire of proteins secreted by the type III secretion apparatus of Shigella flexneri. *Mol Microbiol* **38**, 760-771 (2000).
26. J. M. Hansen *et al.*, Pathogenic ubiquitination of GSDMB inhibits NK cell bactericidal functions. *Cell* **184**, 3178-3191.e3118 (2021).
27. C. Wang *et al.*, Structural basis for GSDMB pore formation and its targeting by IpaH7.8. *Nature* **616**, 590-597 (2023).
28. G. Luchetti *et al.*, Shigella ubiquitin ligase IpaH7.8 targets gasdermin D for degradation to prevent pyroptosis and enable infection. *Cell Host Microbe* **29**, 1521-1530.e1510 (2021).
29. M. F. de Jong, Z. Liu, D. Chen, N. M. Alto, Shigella flexneri suppresses NF-κB activation by inhibiting linear ubiquitin chain ligation. *Nat Microbiol* **1**, 16084 (2016).
30. J. Liu *et al.*, Mechanistic insights into the subversion of the linear ubiquitin chain assembly complex by the E3 ligase IpaH1.4 of. *Proc Natl Acad Sci U S A* **119**, e2116776119 (2022).
31. T. Sanada *et al.*, The Shigella flexneri effector OspI deamidates UBC13 to dampen the inflammatory response. *Nature* **483**, 623-626 (2012).
32. X. Mou, S. Souter, J. Du, A. Z. Reeves, C. F. Lesser, Synthetic bottom-up approach reveals the complex interplay of. *Proc Natl Acad Sci U S A* **115**, 6452-6457 (2018).
33. J. D. Ballard, R. J. Collier, M. N. Starnbach, Anthrax toxin-mediated delivery of a cytotoxic T-cell epitope in vivo. *Proc Natl Acad Sci U S A* **93**, 12531-12534 (1996).
34. I. Rauch *et al.*, NAIP proteins are required for cytosolic detection of specific bacterial ligands in vivo. *J Exp Med* **213**, 657-665 (2016).
35. Y. Zhu *et al.*, Structural insights into the enzymatic mechanism of the pathogenic MAPK phosphothreonine lyase. *Mol Cell* **28**, 899-913 (2007).
36. L. Chen *et al.*, Structural basis for the catalytic mechanism of phosphothreonine lyase. *Nat Struct Mol Biol* **15**, 101-102 (2008).
37. N. S. Duesbery *et al.*, Proteolytic inactivation of MAP-kinase-kinase by anthrax lethal factor. *Science* **280**, 734-737 (1998).
38. G. Vitale *et al.*, Anthrax lethal factor cleaves the N-terminus of MAPKKs and induces tyrosine/threonine phosphorylation of MAPKs in cultured macrophages. *Biochem Biophys Res Commun* **248**, 706-711 (1998).

bioRxiv preprint doi: https://doi.org/10.1101/2025.02.01.636075; this version posted February 2, 2025. The copyright holder for this preprint (which was not certified by peer review) is the author/funder, who has granted bioRxiv a license to display the preprint in perpetuity. It is made available under aCC-BY-NC-ND 4.0 International license.

39. A. P. Chopra, S. A. Boone, X. Liang, N. S. Duesbery, Anthrax lethal factor proteolysis and inactivation of MAPK kinase. *J Biol Chem* **278**, 9402-9406 (2003).
40. A. J. Bardwell, M. Abdollahi, L. Bardwell, Anthrax lethal factor-cleavage products of MAPK (mitogen-activated protein kinase) kinases exhibit reduced binding to their cognate MAPKs. *Biochem J* **378**, 569-577 (2004).
41. T. Kawai, S. Akira, The role of pattern-recognition receptors in innate immunity: update on Toll-like receptors. *Nat Immunol* **11**, 373-384 (2010).
42. R. G. Gaudet *et al.*, Innate Recognition of Intracellular Bacterial Growth Is Driven by the TIFA-Dependent Cytosolic Surveillance Pathway. *Cell Rep* **19**, 1418-1430 (2017).
43. M. Milivojevic *et al.*, ALPK1 controls TIFA/TRAF6-dependent innate immunity against heptose-1,7-bisphosphate of gram-negative bacteria. *PLoS Pathog* **13**, e1006224 (2017).
44. P. Zhou *et al.*, Alpha-kinase 1 is a cytosolic innate immune receptor for bacterial ADP-heptose. *Nature* **561**, 122-126 (2018).
45. S. E. Girardin *et al.*, CARD4/Nod1 mediates NF-kappaB and JNK activation by invasive Shigella flexneri. *EMBO Rep* **2**, 736-742 (2001).
46. C. Juliana *et al.*, Non-transcriptional priming and deubiquitination regulate NLRP3 inflammasome activation. *J Biol Chem* **287**, 36617-36622 (2012).
47. T. Fernandes-Alnemri *et al.*, Cutting edge: TLR signaling licenses IRAK1 for rapid activation of the NLRP3 inflammasome. *J Immunol* **191**, 3995-3999 (2013).
48. K. M. Lin *et al.*, IRAK-1 bypasses priming and directly links TLRs to rapid NLRP3 inflammasome activation. *Proc Natl Acad Sci U S A* **111**, 775-780 (2014).
49. N. Song *et al.*, NLRP3 Phosphorylation Is an Essential Priming Event for Inflammasome Activation. *Mol Cell* **68**, 185-197.e186 (2017).
50. S. M. Man *et al.*, Inflammasome activation causes dual recruitment of NLRC4 and NLRP3 to the same macromolecular complex. *Proc Natl Acad Sci U S A* **111**, 7403-7408 (2014).
51. J. P. Grayczyk *et al.*, TLR priming licenses NAIP inflammasome activation by immunoevasive ligands. *Proc Natl Acad Sci U S A* **121**, e2412700121 (2024).
52. J. Yang, Z. Liu, T. S. Xiao, Post-translational regulation of inflammasomes. *Cell Mol Immunol* **14**, 65-79 (2017).
53. H. Hara *et al.*, Phosphorylation of the adaptor ASC acts as a molecular switch that controls the formation of speck-like aggregates and inflammasome activity. *Nat Immunol* **14**, 1247-1255 (2013).
54. Y. C. Lin *et al.*, Syk is involved in NLRP3 inflammasome-mediated caspase-1 activation through adaptor ASC phosphorylation and enhanced oligomerization. *J Leukoc Biol* **97**, 825-835 (2015).
55. I. C. Chung *et al.*, Pyk2 activates the NLRP3 inflammasome by directly phosphorylating ASC and contributes to inflammasome-dependent peritonitis. *Sci Rep* **6**, 36214 (2016).
56. M. A. Gavrilin, E. R. Prather, A. D. Vompe, C. C. McAndrew, M. D. Wewers, cAbl Kinase Regulates Inflammasome Activation and Pyroptosis via ASC Phosphorylation. *J Immunol* **206**, 1329-1336 (2021).
57. J. Kortmann, S. W. Brubaker, D. M. Monack, Cutting Edge: Inflammasome Activation in Primary Human Macrophages Is Dependent on Flagellin. *J Immunol* **195**, 815-819 (2015).
58. M. Rayamajhi, D. E. Zak, J. Chavarria-Smith, R. E. Vance, E. A. Miao, Cutting edge: Mouse NAIP1 detects the type III secretion system needle protein. *J Immunol* **191**, 3986-3989 (2013).
59. Y. Qu *et al.*, Phosphorylation of NLRC4 is critical for inflammasome activation. *Nature* **490**, 539-542 (2012).

bioRxiv preprint doi: https://doi.org/10.1101/2025.02.01.636075; this version posted February 2, 2025. The copyright holder for this preprint (which was not certified by peer review) is the author/funder, who has granted bioRxiv a license to display the preprint in perpetuity. It is made available under aCC-BY-NC-ND 4.0 International license.

60. M. Matusiak *et al.*, Flagellin-induced NLRC4 phosphorylation primes the inflammasome for activation by NAIP5. *Proc Natl Acad Sci U S A* **112**, 1541-1546 (2015).
61. W. Liu *et al.*, LRRK2 promotes the activation of NLRC4 inflammasome during. *J Exp Med* **214**, 3051-3066 (2017).
62. J. L. Tenthorey *et al.*, NLRC4 inflammasome activation is NLRP3- and phosphorylation-independent during infection and does not protect from melanoma. *J Exp Med* **217**, (2020).
63. M. F. Mohamed *et al.*, CrkII/Abl phosphorylation cascade is critical for NLRC4 inflammasome activity and is blocked by Pseudomonas aeruginosa ExoT. *Nat Commun* **13**, 1295 (2022).
64. S. Suzuki *et al.*, Shigella type III secretion protein MxiI is recognized by Naip2 to induce Nlrc4 inflammasome activation independently of Pkcδ. *PLoS Pathog* **10**, e1003926 (2014).
65. J. L. Poyet *et al.*, Identification of Ipaf, a human caspase-1-activating protein related to Apaf-1. *J Biol Chem* **276**, 28309-28313 (2001).
66. T. Suzuki *et al.*, Differential regulation of caspase-1 activation, pyroptosis, and autophagy via Ipaf and ASC in Shigella-infected macrophages. *PLoS Pathog* **3**, e111 (2007).
67. C. L. Case, S. Shin, C. R. Roy, Asc and Ipaf Inflammasomes direct distinct pathways for caspase-1 activation in response to Legionella pneumophila. *Infect Immun* **77**, 1981-1991 (2009).
68. P. Broz *et al.*, Redundant roles for inflammasome receptors NLRP3 and NLRC4 in host defense against Salmonella. *J Exp Med* **207**, 1745-1755 (2010).
69. P. Broz, J. von Moltke, J. W. Jones, R. E. Vance, D. M. Monack, Differential requirement for Caspase-1 autoproteolysis in pathogen-induced cell death and cytokine processing. *Cell Host Microbe* **8**, 471-483 (2010).
70. D. Bierschenk *et al.*, The Salmonella pathogenicity island-2 subverts human NLRP3 and NLRC4 inflammasome responses. *J Leukoc Biol* **105**, 401-410 (2019).
71. F. Moghaddas *et al.*, Autoinflammatory mutation in NLRC4 reveals a leucine-rich repeat (LRR)-LRR oligomerization interface. *J Allergy Clin Immunol* **142**, 1956-1967.e1956 (2018).
72. J. L. Roncaioli *et al.*, A hierarchy of cell death pathways confers layered resistance to shigellosis in mice. *Elife* **12**, (2023).
73. S. Nordlander, J. Pott, K. J. Maloy, NLRC4 expression in intestinal epithelial cells mediates protection against an enteric pathogen. *Mucosal Immunol* **7**, 775-785 (2014).
74. M. E. Sellin *et al.*, Epithelium-intrinsic NAIP/NLRC4 inflammasome drives infected enterocyte expulsion to restrict Salmonella replication in the intestinal mucosa. *Cell Host Microbe* **16**, 237-248 (2014).
75. I. Rauch *et al.*, NAIP-NLRC4 Inflammasomes Coordinate Intestinal Epithelial Cell Expulsion with Eicosanoid and IL-18 Release via Activation of Caspase-1 and -8. *Immunity* **46**, 649-659 (2017).
76. A. Hausmann *et al.*, Intestinal epithelial NAIP/NLRC4 restricts systemic dissemination of the adapted pathogen Salmonella Typhimurium due to site-specific bacterial PAMP expression. *Mucosal Immunol* **13**, 530-544 (2020).
77. P. Samperio Ventayol *et al.*, Bacterial detection by NAIP/NLRC4 elicits prompt contractions of intestinal epithelial cell layers. *Proc Natl Acad Sci U S A* **118**, (2021).
78. N. Romberg *et al.*, Mutation of NLRC4 causes a syndrome of enterocolitis and autoinflammation. *Nat Genet* **46**, 1135-1139 (2014).
79. S. W. Canna *et al.*, An activating NLRC4 inflammasome mutation causes autoinflammation with recurrent macrophage activation syndrome. *Nat Genet* **46**, 1140-1146 (2014).

bioRxiv preprint doi: https://doi.org/10.1101/2025.02.01.636075; this version posted February 2, 2025. The copyright holder for this preprint (which was not certified by peer review) is the author/funder, who has granted bioRxiv a license to display the preprint in perpetuity. It is made available under aCC-BY-NC-ND 4.0 International license.

80. J. Liang *et al.*, Novel NLRC4 Mutation Causes a Syndrome of Perinatal Autoinflammation With Hemophagocytic Lymphohistiocytosis, Hepatosplenomegaly, Fetal Thrombotic Vasculopathy, and Congenital Anemia and Ascites. *Pediatr Dev Pathol* **20**, 498-505 (2017).
81. S. W. Canna *et al.*, Life-threatening NLRC4-associated hyperinflammation successfully treated with IL-18 inhibition. *J Allergy Clin Immunol* **139**, 1698-1701 (2017).
82. K. Asna Ashari *et al.*, Three cases of autoinflammatory disease with novel NLRC4 mutations, and the first mutation reported in the CARD domain of NLRC4 associated with autoinflammatory infantile enterocolitis (AIFEC). *Pediatr Rheumatol Online J* **22**, 90 (2024).
83. A. T. Maurelli, B. Blackmon, R. Curtiss, Loss of pigmentation in Shigella flexneri 2a is correlated with loss of virulence and virulence-associated plasmid. *Infect Immun* **43**, 397-401 (1984).
84. T. Schmidt, J. L. Schmid-Burgk, V. Hornung, Synthesis of an arrayed sgRNA library targeting the human genome. *Sci Rep* **5**, 14987 (2015).
85. K. Labun *et al.*, CHOPCHOP v3: expanding the CRISPR web toolbox beyond genome editing. *Nucleic Acids Res* **47**, W171-W174 (2019).

bioRxiv preprint doi: https://doi.org/10.1101/2025.02.01.636075; this version posted February 2, 2025. The copyright holder for this preprint (which was not certified by peer review) is the author/funder, who has granted bioRxiv a license to display the preprint in perpetuity. It is made available under aCC-BY-NC-ND 4.0 International license.

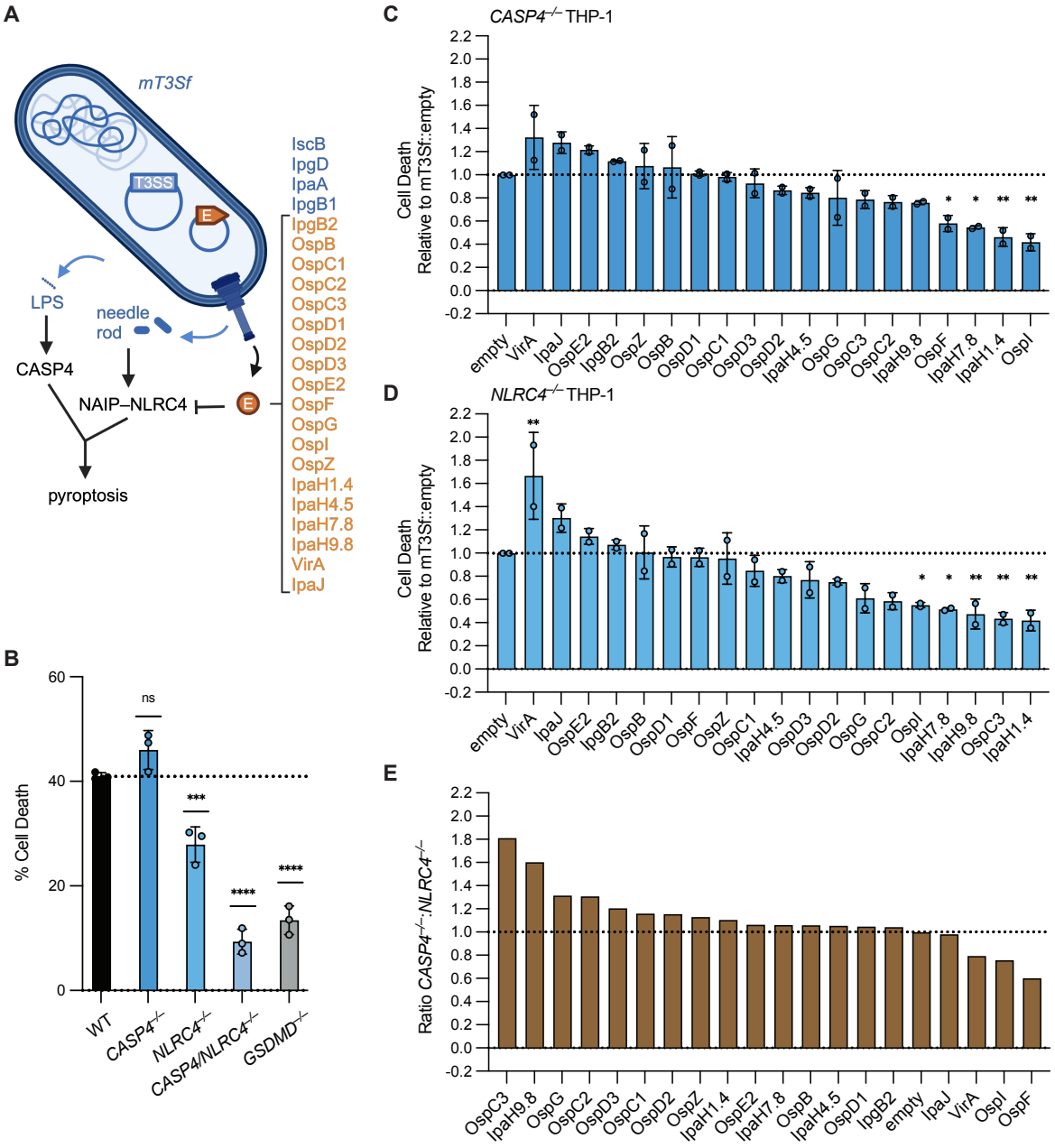

Figure 1. A mT3Sf screen identifies OspF as a specific suppressor of the NAIP–NLRC4 inflammasome. A. mT3Sf model. Features of mT3Sf::empty shown in dark blue with type III secretion system ("T3SS"). Individual effectors ("E") introduced shown in orange. Created with BioRender.com. **B.** WT, *CASP4*$^{-/-}$, *NLRC4*$^{-/-}$, *CASP4/NLRC4*$^{-/-}$, or *GSDMD*$^{-/-}$ THP-1 cells infected with mT3Sf::empty at an MOI of 5. Cell death was measured at 1 hpi by propidium iodide uptake and calculated as % Cell Death relative to TritonX-100 treatment. **C.** *CASP4*$^{-/-}$ or **D.** *NLRC4*$^{-/-}$ THP-1 cells infected with mT3Sf strains at an MOI of 5 for 2 hr. Percent Cell Death calculated as in B. Data shows cell death relative to mT3Sf::empty infection. **E.** Ratio of *CASP4*$^{-/-}$*:NLRC4*$^{-/-}$ normalized cell death from C and D. Data are representative of at least three independent experiments, each with three technical replicates, and shown as mean ± SD in B.

bioRxiv preprint doi: https://doi.org/10.1101/2025.02.01.636075; this version posted February 2, 2025. The copyright holder for this preprint (which was not certified by peer review) is the author/funder, who has granted bioRxiv a license to display the preprint in perpetuity. It is made available under aCC-BY-NC-ND 4.0 International license.

For C and D, data represent the mean ± SD of two experimental repeats, each with three technical replicates. One-way ANOVA. **P < 0.0332, **P < 0.0021, ***P < 0.0002*, *****P < 0.0001*.

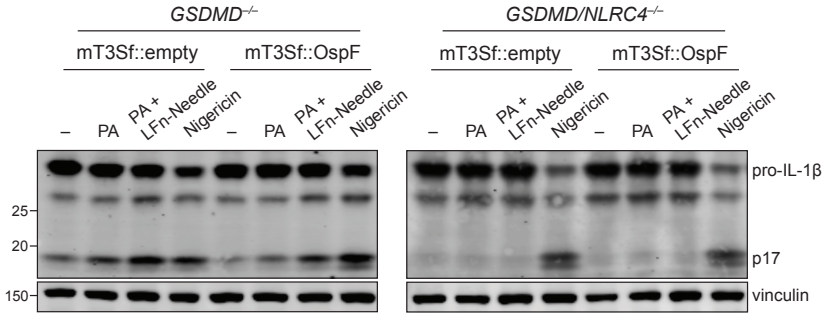

Supplemental Figure 1. mT3Sf::OspF infection suppresses NLRC4-dependent IL-1β processing. Western Blot of lysates from *GSDMD*$^{-/-}$ or *GSDMD/NLRC4*$^{-/-}$ THP-1 cells infected at MOI 5 with mT3Sf::empty or mT3Sf::OspF for 1 hr before challenge with PA, PA + LFn-Needle, Nigericin, or left unchallenged for 2 hr.

bioRxiv preprint doi: https://doi.org/10.1101/2025.02.01.636075; this version posted February 2, 2025. The copyright holder for this preprint (which was not certified by peer review) is the author/funder, who has granted bioRxiv a license to display the preprint in perpetuity. It is made available under aCC-BY-NC-ND 4.0 International license.

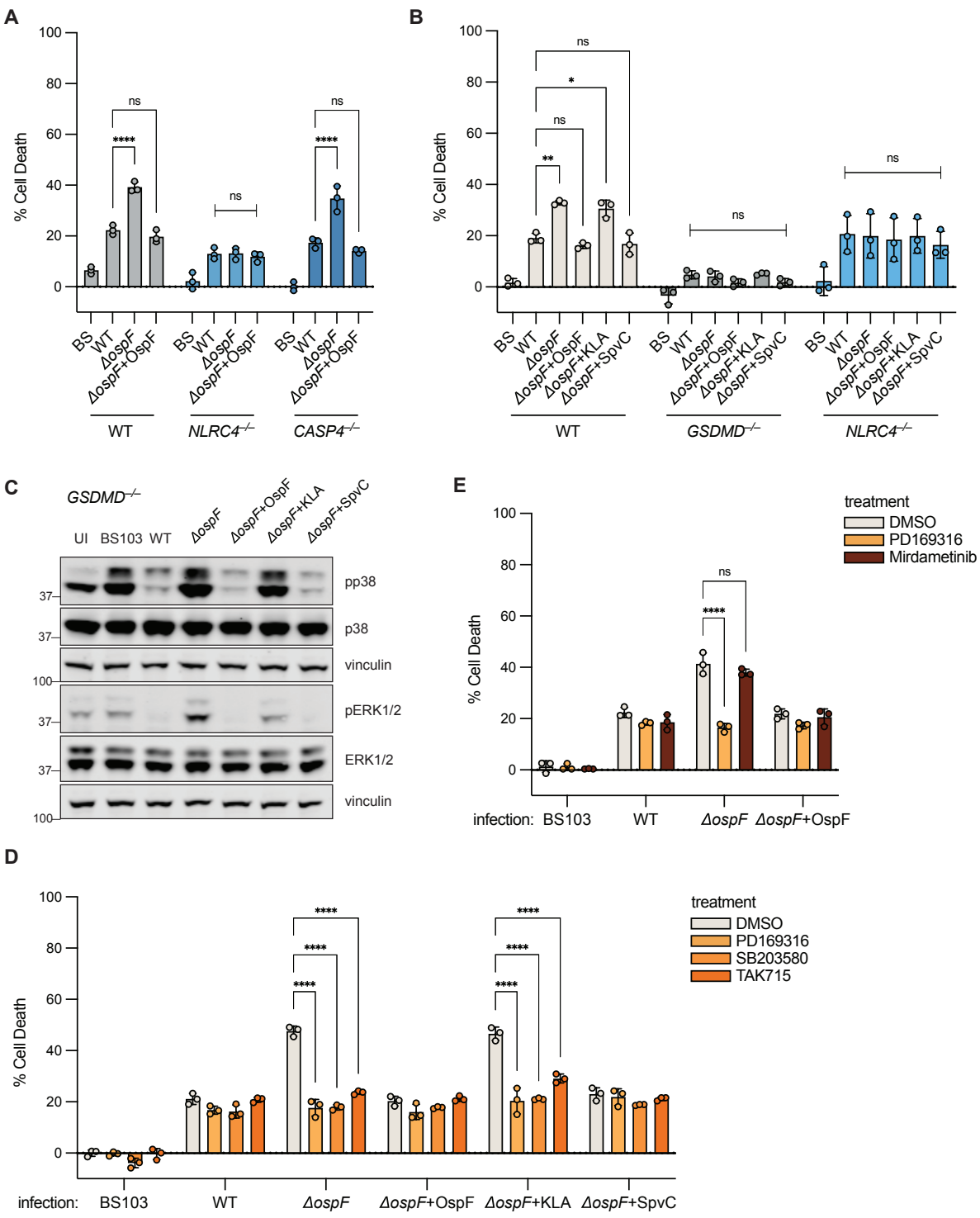

Figure 2. OspF suppresses the NAIP–NLRC4 inflammasome during *Shigella* infection via p38 inactivation in human cells. A. WT, *NLRC4*$^{-/-}$, or *CASP4*$^{-/-}$ THP-1 cells infected with *Shigella flexneri* at an MOI of 10. **B.** WT, *GSDMD*$^{-/-}$, or *NLRC4*$^{-/-}$ THP-1 cells infected with *Shigella flexneri* at an MOI of 10. **C.** Western Blot of lysates from *Shigella*-infected *GSDMD*$^{-/-}$ THP-1 cells, collected at 1 hpi. **D.** WT THP-1 cells pre-treated for 1 hr with DMSO or p38 inhibitors, 5 μM PD169316, 5 μM SB203580, or 5 μM TAK715 before infection with *Shigella*. **E.**

bioRxiv preprint doi: https://doi.org/10.1101/2025.02.01.636075; this version posted February 2, 2025. The copyright holder for this preprint (which was not certified by peer review) is the author/funder, who has granted bioRxiv a license to display the preprint in perpetuity. It is made available under aCC-BY-NC-ND 4.0 International license.

WT THP-1 cells treated pre-treated for 1 hr with DMSO, 5 μM PD169316 or 5 μM Mirdametinib before infection with *Shigella*. Data are representative of at least three independent experiments, each with three technical replicates. Cell death was measured at 1 hpi by propidium iodide uptake and calculated as % Cell Death relative to TritonX-100 treatment. Data represent the mean ± SD. Two-way ANOVA. **P < 0.0332, **P < 0.0021, ***P < 0.0002*, *****P < 0.0001* (A-B, D-E).

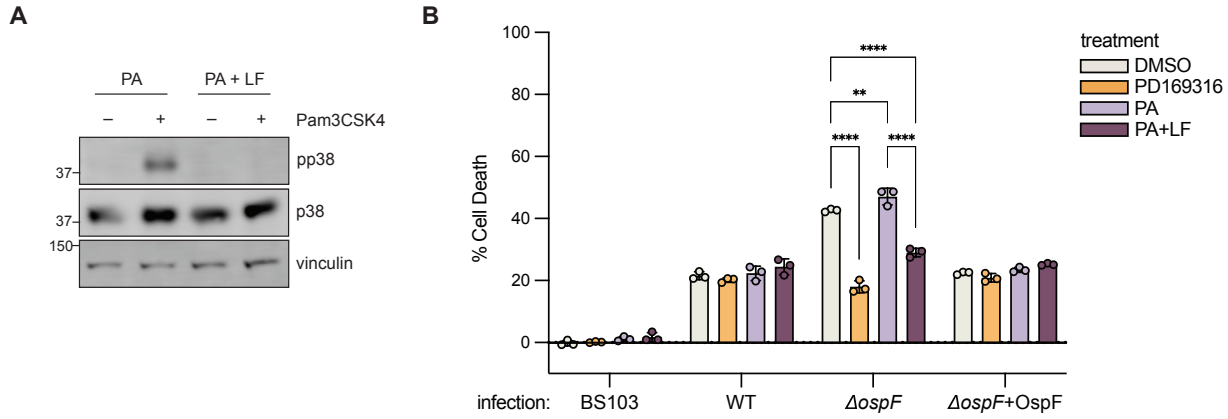

Supplemental Figure 2. Lethal Factor inactivation of MKKs suppresses NLRC4-dependent cell death during *ΔospF* infection. A. Western Blot of lysates from WT THP-1 cells treated with PA or PA + Lethal Factor (LF) for 1 hr before priming with 100 ng/mL Pam3CSK4 for 1 hr. **B.** WT THP-1 cells treated pre-treated for 1 hr with DMSO, 5 μM PD169316, PA, or PA + LF before infection with *Shigella* at an MOI of 10. Data are representative of at least three independent experiments, each with three technical replicates. Cell death was measured at 1hpi by propidium iodide uptake and calculated as % Cell Death relative to TritonX-100 treatment. Data represent the mean ± SD. Two-way ANOVA. **P < 0.0332, **P < 0.0021, ***P < 0.0002*, *****P < 0.0001* (A-B, D-E).

bioRxiv preprint doi: https://doi.org/10.1101/2025.02.01.636075; this version posted February 2, 2025. The copyright holder for this preprint (which was not certified by peer review) is the author/funder, who has granted bioRxiv a license to display the preprint in perpetuity. It is made available under aCC-BY-NC-ND 4.0 International license.

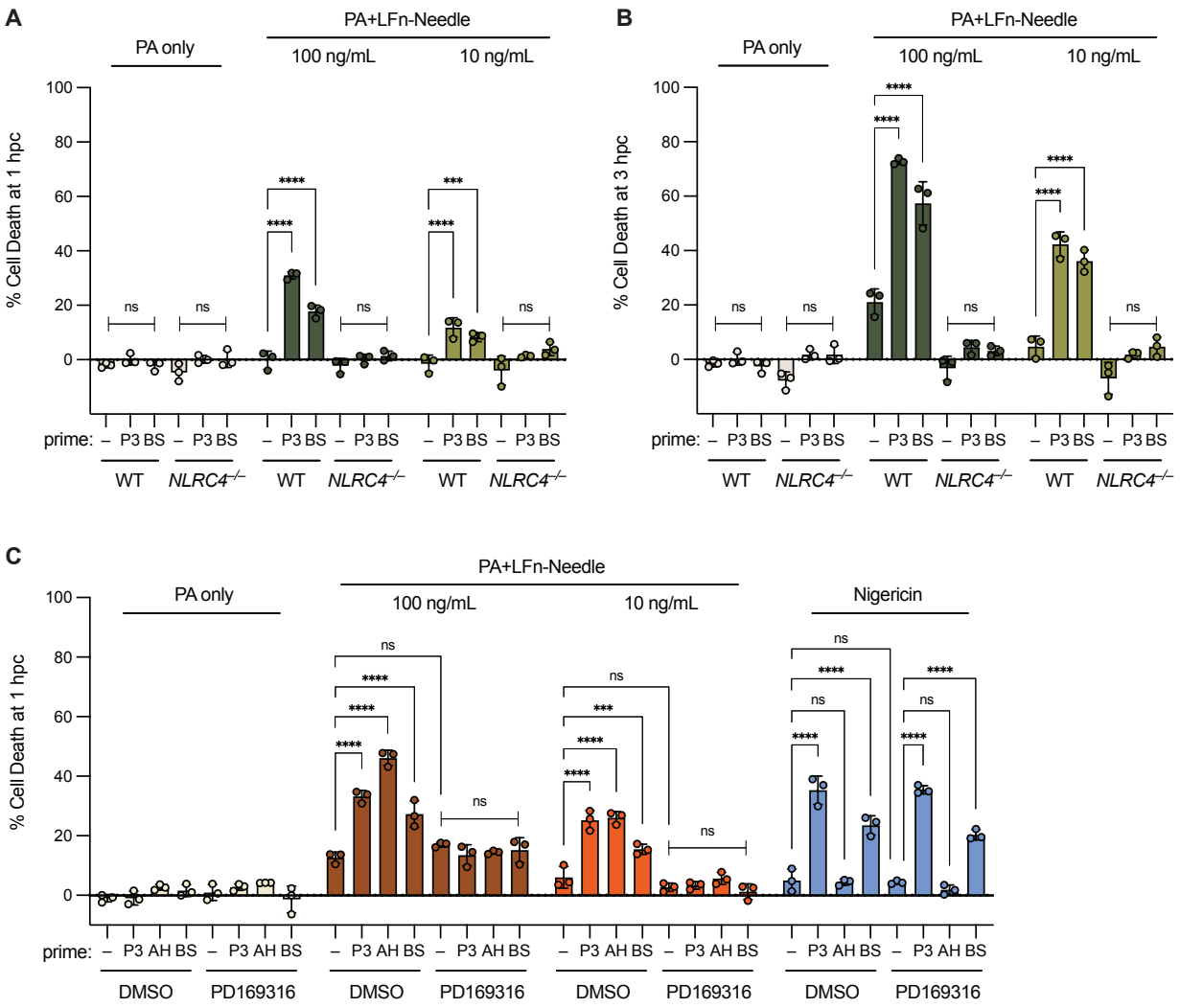

Figure 3. Rapid priming sensitizes the NAIP–NLRC4 inflammasome in a p38-dependent manner. A. and **B.** WT or *NLRC4*$^{-/-}$ THP-1 cells primed for 1 hr with 100 ng/mL Pam3CSK4 (P3) or BS103 at MOI 10 (BS) before challenge with PA or PA+LFn-Needle. Cell death collected at 1 hpc (A), and 3 hpc (B). **C.** WT THP-1 cells pre-treated for 1 hr with DMSO or 5 μM PD169316, and primed for 1 hr with 100 ng/mL Pam3CSK4 (P3), 100 ng/mL ADP-L-Heptose (AH), or BS103 at MOI 10 (BS) before challenge with PA, PA+LFn-Needle, or 5 μg/mL Nigericin. Data are representative of at least three independent experiments, each with three technical replicates. Cell death was measured at 1 hpc or 3 hpc by propidium iodide uptake and calculated as % Cell Death relative to TritonX-100 treatment. Data represent the mean ± SD. Two-way ANOVA. **P < 0.0332, **P < 0.0021, ***P < 0.0002*, *****P < 0.0001.*

bioRxiv preprint doi: https://doi.org/10.1101/2025.02.01.636075; this version posted February 2, 2025. The copyright holder for this preprint (which was not certified by peer review) is the author/funder, who has granted bioRxiv a license to display the preprint in perpetuity. It is made available under aCC-BY-NC-ND 4.0 International license.

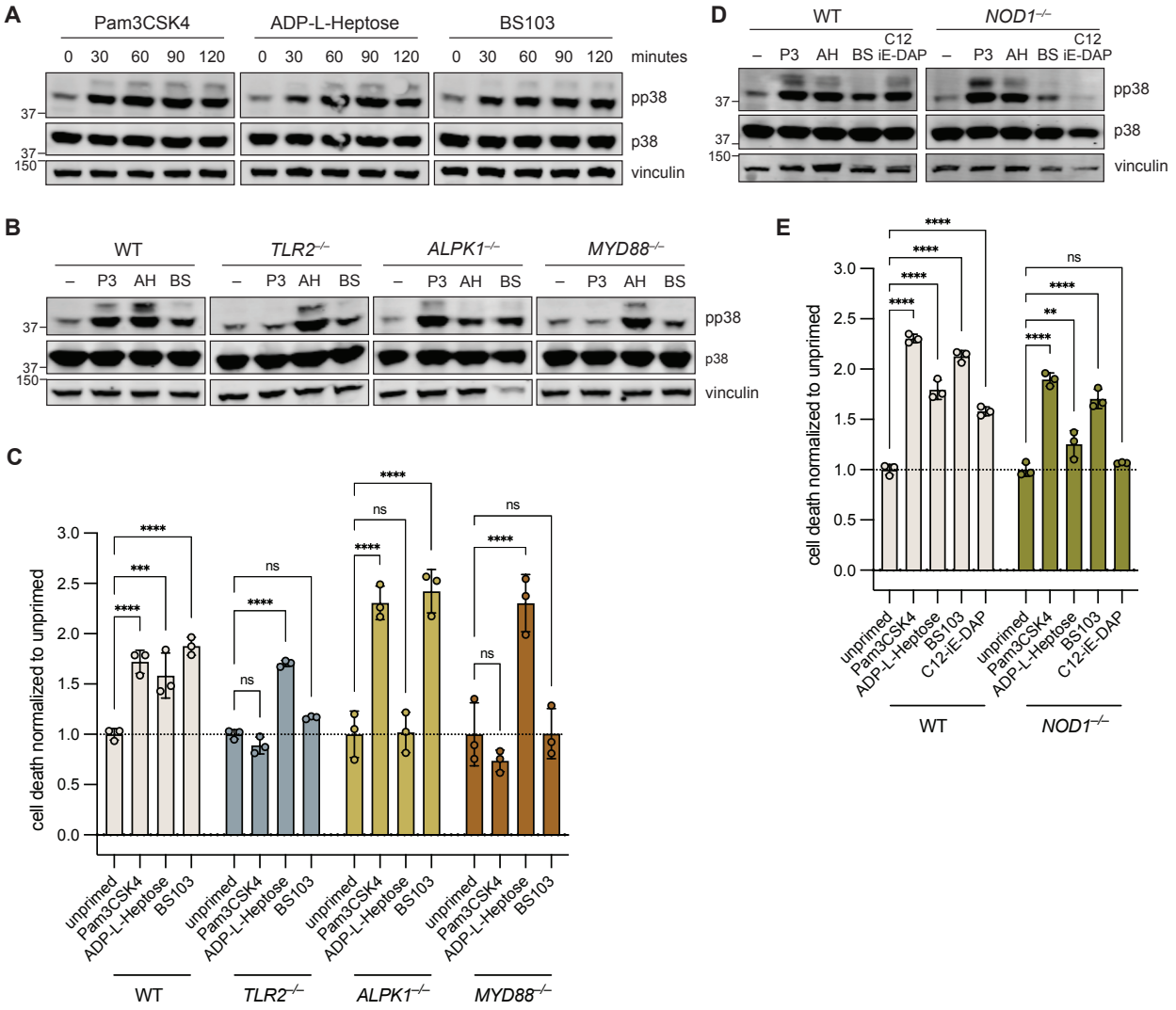

Supplemental Figure 3. TLR2, ALPK1, and NOD1 activation can prime NAIP–NLRC4. A. Western Blot of lysates from priming timecourse of WT THP-1 treated with Pam3CSK4, ADP-L-Heptose, or BS103. **B.** and **C.** THP-1 knockout validation of *TLR2*, *ALPK1*, and *MYD88*$^{-/-}$ THP-1 cells for priming induced phospho-p38 (pp38) (B), and enhanced response to NeedleTox challenge (C). **D.** and **E.** THP-1 knockout validation of *NOD1*$^{-/-}$ THP-1s for priming induced pp38 (D), and enhanced response to NeedleTox challenge (E). C and E Cell death was measured at 3 hpc by propidium iodide uptake and calculated as % Cell Death relative to TritonX-100 treatment. Fold change of cell death of primed cells relative to unprimed cells, all treated with NeedleTox. Data represent the mean ± SD. Two-way ANOVA. **P < 0.0332, **P < 0.0021, ***P < 0.0002*, *****P < 0.0001.*

bioRxiv preprint doi: https://doi.org/10.1101/2025.02.01.636075; this version posted February 2, 2025. The copyright holder for this preprint (which was not certified by peer review) is the author/funder, who has granted bioRxiv a license to display the preprint in perpetuity. It is made available under aCC-BY-NC-ND 4.0 International license.

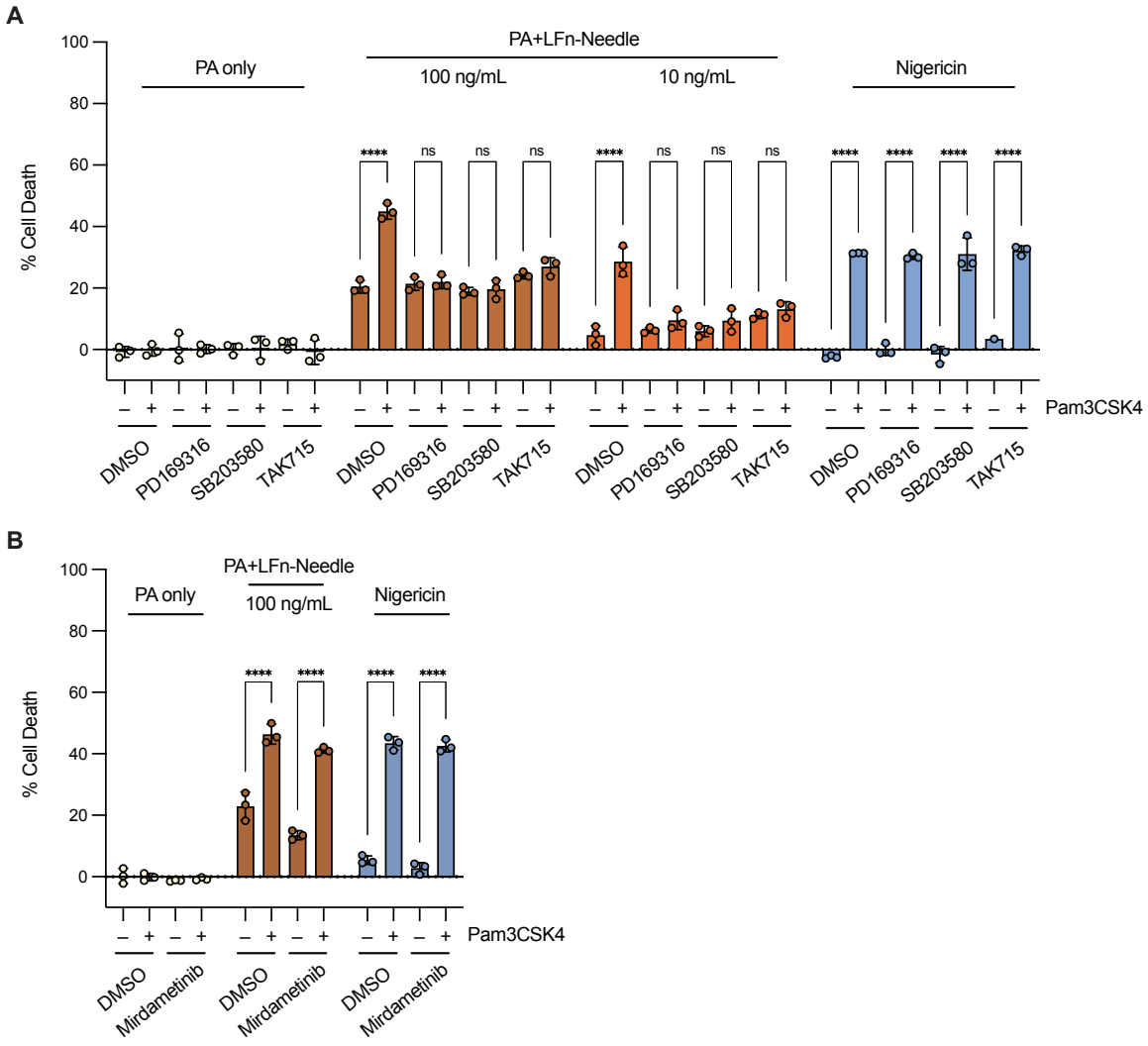

Supplemental Figure 4. p38 inhibitors suppress rapid priming of NAIP–NLRC4. A. WT THP-1 cells pre-treated for 1 hr with DMSO or p38 inhibitors, 5 μM PD169316, 5 μM SB203580, or 5 μM TAK715 before challenge with PA, PA+LFn-Needle, or 5 μg/mL Nigericin. **B.** WT THP-1 cells pre-treated for 1 hr with DMSO or 5 μM MEK1/2 inhibitor mirdametinib before challenge with PA, PA+LFn-Needle, or 5 μg/mL Nigericin. Data are representative of at least three independent experiments, each with three technical replicates. Cell death was measured at 3 hpc by propidium iodide uptake and calculated as % Cell Death relative to TritonX-100 treatment. Data represent the mean ± SD. Two-way ANOVA. **P < 0.0332, **P < 0.0021, ***P < 0.0002*, *****P < 0.0001.*

bioRxiv preprint doi: https://doi.org/10.1101/2025.02.01.636075; this version posted February 2, 2025. The copyright holder for this preprint (which was not certified by peer review) is the author/funder, who has granted bioRxiv a license to display the preprint in perpetuity. It is made available under aCC-BY-NC-ND 4.0 International license.

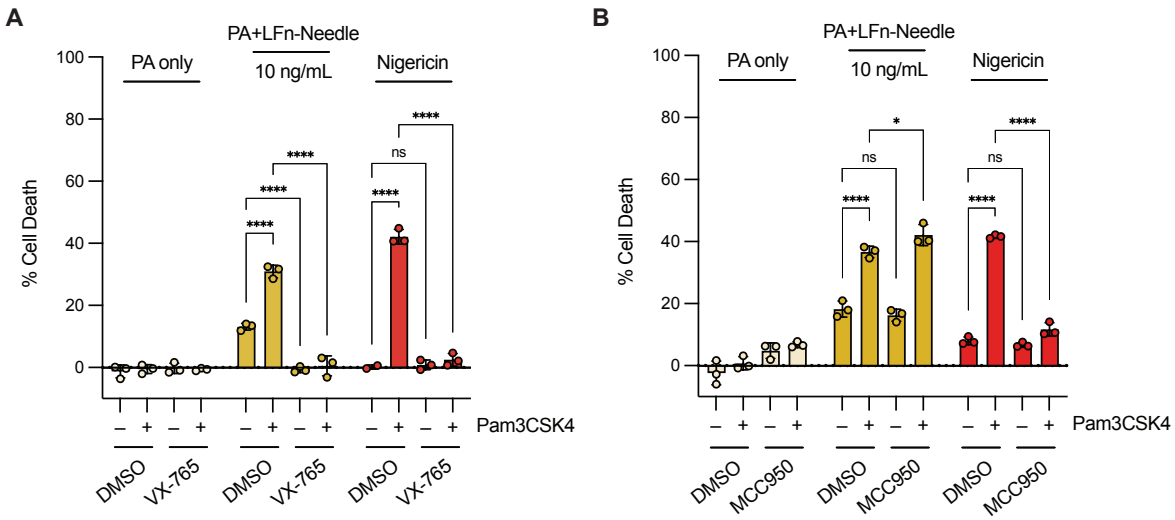

Supplemental Figure 5. Priming of NAIP–NLRC4 is CASP1- and NLRP3-independent. A. WT THP-1 cells pre-treated for 1 hr with DMSO or 20 μM Caspase-1 inhibitor VX-765 before challenge with PA, PA+LFn-Needle, or 5 μg/mL Nigericin. **B.** WT THP-1 cells pre-treated for 1 hr with DMSO or 10 μM NLRP3 inhibitor MCC950 before Pam3CSK4 prime for 1 hr and challenge with PA, PA+LFn-Needle, or 5 μg/mL Nigericin. Data are representative of at least three independent experiments, each with three technical replicates. Cell death was measured at 3 hpi by propidium iodide uptake and calculated as % Cell Death relative to TritonX-100 treatment. Data represent the mean ± SD. Two-way ANOVA. **P < 0.0332, **P < 0.0021, ***P < 0.0002*, *****P < 0.0001* (A).

bioRxiv preprint doi: https://doi.org/10.1101/2025.02.01.636075; this version posted February 2, 2025. The copyright holder for this preprint (which was not certified by peer review) is the author/funder, who has granted bioRxiv a license to display the preprint in perpetuity. It is made available under aCC-BY-NC-ND 4.0 International license.

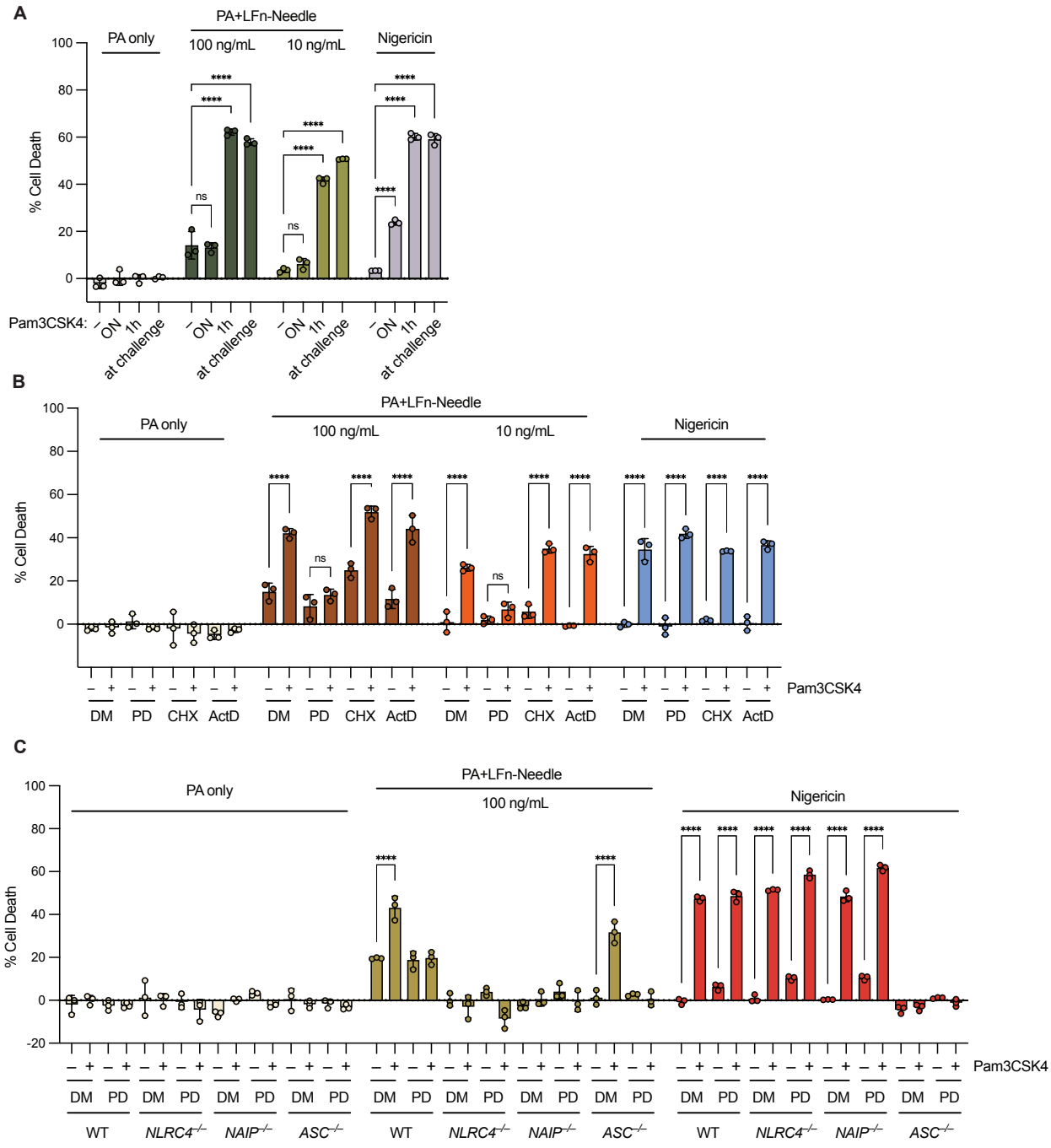

Figure 4. Rapid priming enhances NAIP–NLRC4 activation in a transcription- and translation-independent manner and alleviates requirement for ASC. A. WT THP-1 cells primed with 100 ng/mL Pam3CSK4 overnight (ON), for 1 hr before challenge, or at the time of challenge. Cells challenged with PA, PA+LFn-Needle, or 5 µg/mL Nigericin. **B.** WT THP-1 cells pre-treated for 1 hr with DMSO (DM), 5 µM PD169316 (PD), 250 ng/mL cycloheximide (CHX), or 2 µg/mL actinomycin D (ActD), and primed for 1 hr with 100ng/mL Pam3CSK4 before challenge with PA, PA+LFn-Needle, or 5 µg/mL Nigericin. **C.** WT, *NLRC4*$^{-/-}$, *NAIP*$^{-/-}$, or *ASC*$^{-/-}$ THP-1 cells pre-treated for 1 hr with DMSO or 5 µM PD169316, and primed for 1 hr with 100 ng/mL Pam3CSK4 before challenge with PA or PA+LFn-Needle, or 5 µg/mL Nigericin. Data are

bioRxiv preprint doi: https://doi.org/10.1101/2025.02.01.636075; this version posted February 2, 2025. The copyright holder for this preprint (which was not certified by peer review) is the author/funder, who has granted bioRxiv a license to display the preprint in perpetuity. It is made available under aCC-BY-NC-ND 4.0 International license.

representative of at least three independent experiments, each with three technical replicates. Cell death was measured or 3 hpc by propidium iodide uptake and calculated as % Cell Death relative to TritonX-100 treatment. Data represent the mean ± SD. Two-way ANOVA. **P < 0.0332, **P < 0.0021, ***P < 0.0002, ****P < 0.0001.*

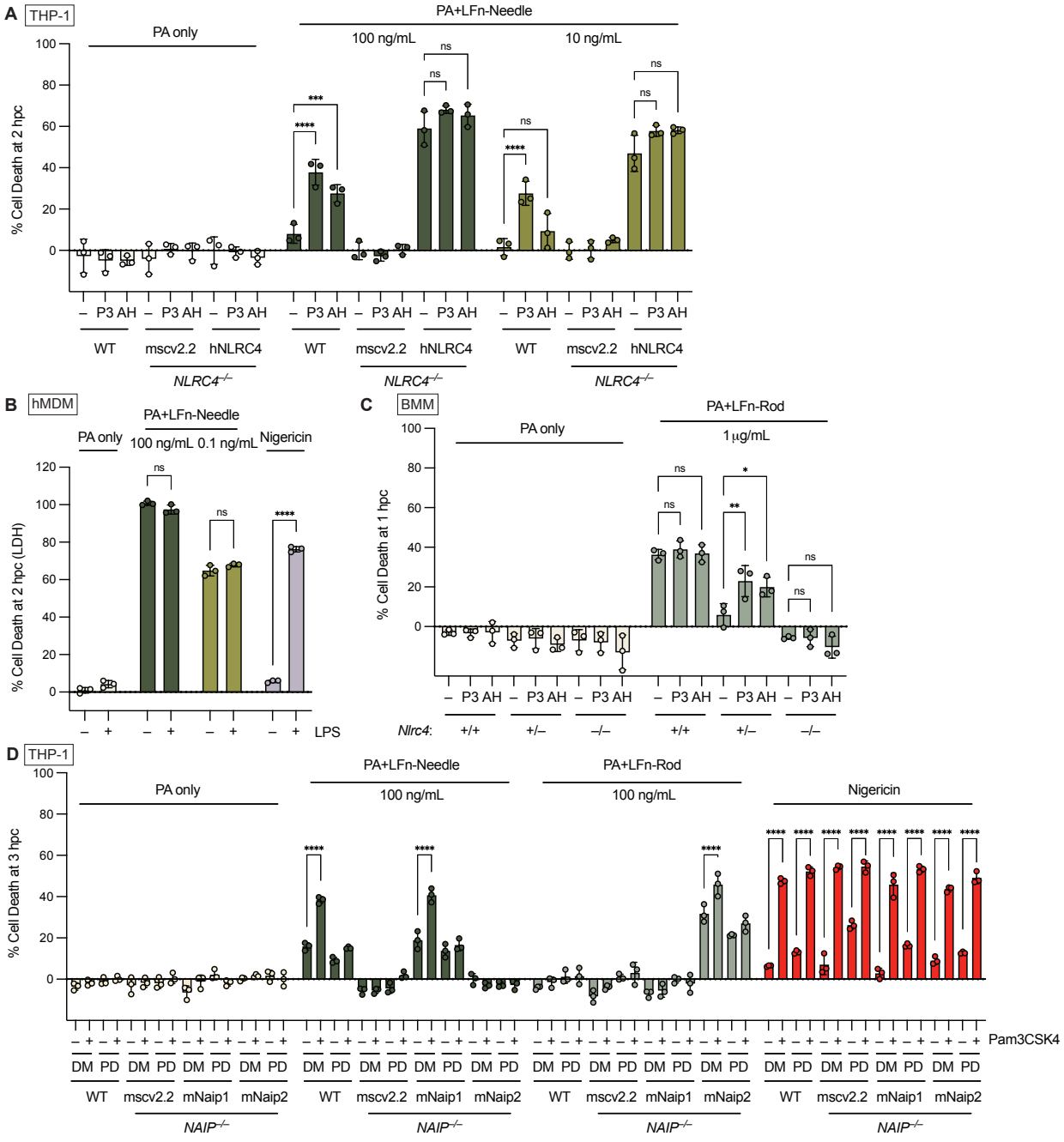

Figure 5. Overexpression of NLRC4, but not NAIP, in THP-1 cells and high expression in primary macrophages masks the priming effect on NAIP–NLRC4. A. WT or transduced *NLRC4*$^{-/-}$ THP-1 cells primed for 1 hr with 100 ng/mL Pam3CSK4 (P3) or 100 ng/mL ADP-L-Heptose (AH) before challenge with PA or PA+LFn-Needle. **B.** Primary human monocyte-

bioRxiv preprint doi: https://doi.org/10.1101/2025.02.01.636075; this version posted February 2, 2025. The copyright holder for this preprint (which was not certified by peer review) is the author/funder, who has granted bioRxiv a license to display the preprint in perpetuity. It is made available under aCC-BY-NC-ND 4.0 International license.

derived macrophages primed for 1 hr with 100 ng/mL LPS before challenge with PA, PA+LFn-Needle, or 5 µg/mL Nigericin. **C.** Mouse bone marrow-derived macrophages primed for 1 hr with 100ng/mL Pam3CSK4 (P3) or 100 ng/mL ADP-L-Heptose (AH) before challenge with PA or PA+LFn-Rod. **D.** WT or transduced *NAIP*$^{-/-}$ THP-1 cells pre-treated for 1 hr with DMSO (DM) or 5 µM PD169316 (PD), and primed for 1 hr with 100 ng/mL Pam3CSK4 before challenge with PA or PA+LFn-Needle, PA+LFn-Rod, or 5 µg/mL Nigericin. Data are representative of at least three independent experiments, each with three technical replicates. Cell death was measured at 1 hpc (C), 2 hpc (A) or 3 hpc (D) by propidium iodide uptake, or by LDH release at 2 hpc (B) and calculated as % Cell Death relative to TritonX-100 treatment. Data represent the mean ± SD. Two-way ANOVA. **P < 0.0332, **P < 0.0021, ***P < 0.0002*, *****P < 0.0001.*

Supplemental Table 1. Bacterial strains used in this study

Name	Description	Source
Shigella flexneri (WT)	*S. flexneri* 2457T	
BS103	*S. flexneri* 2457T virulence plasmid cured	(81)
Δ*ospF*	*S. flexneri* Δ*ospF*	(32)
Δ*ospF*+OspF	*S. flexneri* Δ*ospF* + pAM238-OspF	(32)
Δ*ospF*+KLA	*S. flexneri* Δ*ospF* + pAM238-OspF KLA	this study
Δ*ospF*+SpvC	*S. flexneri* Δ*ospF* + pAM238-SpvC	this study
mT3Sf::empty	mT3Sf + pDSW206-empty	this study
mT3Sf::ospB	mT3Sf + pDSW206-OspB	this study
mT3Sf::ospC1	mT3Sf + pDSW206-OspC1	this study
mT3Sf::ospC2	mT3Sf + pDSW206-OspC2	Kim et al, in prep
mT3Sf::ospC3	mT3Sf + pDSW206-OspC3	Kim et al, in prep
mT3Sf::ospD1	mT3Sf + pDSW206-OspD1	this study
mT3Sf::ospD2	mT3Sf + pDSW206-OspD2	this study
mT3Sf::ospD3	mT3Sf + pDSW206-OspD3	this study
mT3Sf::ospE2	mT3Sf + pDSW206-OspE2	this study
mT3Sf::ospF	mT3Sf + pDSW206-OspF	this study
mT3Sf::ospG	mT3Sf + pDSW206-OspG	this study
mT3Sf::ospI	mT3Sf + pDSW206-OspI	this study
mT3Sf::ospZ	mT3Sf + pDSW206-OspZ	this study
mT3Sf::ipaH1.4	mT3Sf + pDSW206-IpaH1.4	this study
mT3Sf::ipaH4.5	mT3Sf + pDSW206-IpaH4.5	this study
mT3Sf::ipaH7.8	mT3Sf + pDSW206-IpaH7.8	this study
mT3Sf::ipaH9.8	mT3Sf + pDSW206-IpaH9.8	this study
mT3Sf::ipaJ	mT3Sf + pDSW206-IpaJ	this study
mT3Sf::ipgB2	mT3Sf + pDSW206-IpgB2	this study
mT3Sf::virA	mT3Sf + pDSW206-VirA	this study